INVERSE PROBLEM TRANSFORM: SOLVING HYPERSPECTRAL INPAINTING VIA DETERMINISTIC COMPRESSED SENSING

Chia-Hsiang Lin, and Po-Wei Tang

Department of Electrical Engineering, National Cheng Kung University, Tainan, Taiwan
Email: chiahsiang.steven.lin@gmail.com; q36081305@gs.ncku.edu.tw

ABSTRACT

Hyperspectral inpainting (HI) is a challenging inverse problem for reconstructing the image from its incomplete acquisition. Unlike existing methods that solve HI directly, this paper explores a different line of attack by transforming HI into another inverse problem, i.e., decoding in hyperspectral compressed sensing (DHCS). Since HI and DHCS both aim to output the complete hyperspectral data, we can solve HI via DHCS, if we are given an effective DHCS method, and if the required input of such DHCS method can be computed from the observable but incomplete image (OII). Computing the required inputs of most DHCS methods is in general very difficult due to the involved randomness of spectrum projection, so the DHCS method considered here is a deterministic one recently developed for satellite remote sensing. The motivation is that though it is hard to recover the complete image from OII, we found that the input of this deterministic DHCS method can be easily computed from OII. This simple idea of inverse problem transform surprisingly yields completive HI performance.

***Index Terms*—** Inverse problem, hyperspectral image, image inpainting, compressed sensing, inverse problem transform

1. INTRODUCTION

Various spectral, spatial and temporal information embedded in hyperspectral images (HSI) provides valuable analysis for us to observe the Earth's surface, having also found numerous interdisciplinary applications, such as precision agriculture, land cover classification, mineralogy mapping, astronomy and bioinformatics [1–3]. Recently, in the landcover classification field, spectral variability, common subspace learning (CoSpace), and cross-modality learning framework called learnable manifold alignment (LeMA) cooperating with graph learning are considered for hyperspectral analysis techniques [4–6]. Typical HSI spectra range from visible over near-infrared to shortwave infrared bands (from 0.3μm to 2.5 μm), and very recently potential applications of *penetrating* HSI signal in the terahertz bands have also been explored for chemical pellets analysis [7]. However, signals measured by hyperspectral sensors may be corrupted by various noise sources, including random noise and fixed-pattern noise. Processing HSI with fixed-pattern noise (e.g., the widely encountered striped noise in satellite imaging) requires solving the hyperspectral inpainting (HI) problem, which is an inverse problem for reconstructing the HSI from its damaged or incompletely acquired version.

Several benchmark HI techniques have been proposed, including partial differential equation based method (PDE) [8] and sparse Bayesian dictionary learning [9]. A three-dimensional version of PDE (3D-PDE) is also proposed for 3D data in [10], which exploits the information of surrounding areas of some corrupted regions. We should also mention the nonparametric Bayesian method developed based on the Beta-Bernoulli process factor analysis (BPFA) [9, 11]. On the other hand, a low-rank model based method with self-similarity regularizer, termed FastHyIn, has also been proposed for de-striping hyperspectral data [12]. Due to the lack of an explicit definition of self-similarity [13], FastHyIn employs the plug-and-play learning strategy.

In this paper, we approach the HI problem by a radically new method—inverse problem transform (IPT), which reformulates the HI inverse problem into another inverse problem, i.e., decoding in hyperspectral compressed sensing (DHCS). Though it is hard to recover the HSI from the observable but incomplete image (OII),

This work is funded partly by the Young Scholar Fellowship Program (Einstein Program) of Ministry of Science and Technology (MOST) in Taiwan, under Grant MOST 108-2636-E-006-012; and partly by the Higher Education Sprout Project of Ministry of Education (MOE) to the Headquarters of University Advancement at National Cheng Kung University (NCKU).

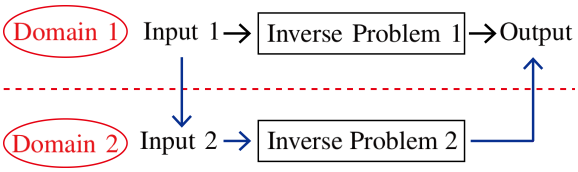

Fig. 1. Graphical illustration of the proposed idea. The two inverse problems (IPs) may have different input quantities, but should have the same target output. To make the transform between the two IPs practically useful, IP 2 should be relatively easy or better studied than IP 1, and the required input of IP 2 should be easily obtained from the input of IP 1.

we found that the input of a recent deterministic DHCS algorithm [14] can be easily computed from OII. Note that the output of such DHCS algorithm (with input available) is exactly the desired output of the HI problem; specifically, both HI and DHCS aim to output the complete HSI data. This simple idea of IPT surprisingly yields completive HI performance, as will be demonstrated experimentally.

Notations: $\boldsymbol{I}_n$ is the $n \times n$ identity matrix. $\boldsymbol{1}_n$ is an n-dimensional all-one vector. $\otimes$ denotes the Kronecker product. $[\boldsymbol{v}]_{a:b}$ is the subvector of $\boldsymbol{v}$ formed by its ath to bth entries. $\mathbb{R}^n$ is the n-dimensional Euclidean space, and $\mathbb{R}^{m\times n}$ is the $m \times n$-dimensional real-valued matrix space. $\mathbb{Z}_{++}$ is the set of all positive integers. $\mathrm{vec}(\cdot)$ is the vectorization operator. The set $\mathcal{I}_Z \triangleq \{1, \ldots, Z\}$ is defined for any given positive integer $Z \in \mathbb{Z}_{++}$.

2. INVERSE PROBLEM TRANSFORM (IPT): CONCEPT AND APPLICATION

2.1. General Framework of IPT

Inverse problem (IP), playing a central role in signal processing, is to compute from observable quantities (input) the causal factors (output) that produced them. In hyperspectral remote sensing, there are many important IPs, including super-resolution [15], unmixing [16, 17], inpainting/denoising [9], and compressed sensing [14]. In hyperspectral inpainting, for example, the input is the incompletely acquired data, from which we want to compute the desired output that is the complete hyperspectral data cube.

Some IPs are considered relatively easy, but some are difficult. As illustrated in Figure 1, if we transform a challenging IP (i.e., IP 1) into an easier or well studied IP (i.e., IP 2), it should be very helpful when the two IPs satisfy the following three conditions:

1. (A1) IP 2 is easier, or can be more effectively solved using available technique.
2. (A2) The input of IP 1 (observable quantity) is sufficient for computing or well approximating the required input of IP 2.
3. (A3) Both IPs aim to recover the same causal factor (i.e., the same target output).

When the considered application scenario satisfies the above three conditions/assumptions, our idea of IP transform is then practically attractive.

2.2. HI Problem Definition and IPT-based Solution

Let us demonstrate the effectiveness of our idea by solving the challenging HI problem (i.e., IP 1 in this work) by transforming it into the DHCS problem (i.e., IP 2 in this work). We begin with defining the HI problem.

Consider an M-band HSI with L pixels $\boldsymbol{x}_1, \ldots, \boldsymbol{x}_L \in \mathbb{R}^M$, which can be ordered into L columns of a matrix $\boldsymbol{X} \triangleq [\boldsymbol{x}_1, \ldots, \boldsymbol{x}_L] \in \mathbb{R}^{M\times L}$ according to their acquisition time [14, Section II.A]. In practice, the HSI $\boldsymbol{X}$ may not be completely acquired; let $\overline{\boldsymbol{\Omega}} \subseteq \{(m, \ell) \mid m \in \mathcal{I}_M,\ \ell \in \mathcal{I}_L\}$ denote the set of indices of those missing data. The HI problem is to recover $\boldsymbol{X}$ (causal factor) from the data $\{[\boldsymbol{X}]_{m,\ell} \mid (m, \ell) \in \boldsymbol{\Omega}\}$ (observable quantity), where $\boldsymbol{\Omega} \triangleq \{(m, \ell) \mid m \in \mathcal{I}_M,\ \ell \in \mathcal{I}_L\} \setminus \overline{\boldsymbol{\Omega}}$ is the set of indices of those successfully acquired data, and "$\setminus$" denotes set difference.

The HI method to be developed is inspired by the following three facts, implying the three conditions discussed in Section 2.1:

1. Very recently, hyperspectral compressed sensing has been solved by a radically new and deterministic approach (without relying on random projection), referred to as spatial/spectral compressed encoder (SPACE) [14] (briefly recalled in Section 2.3), whose corresponding DHCS solver shows state-of-the-art HSI reconstruction performance. This matches (A1).
2. The required input of the adopted DHCS solver is deterministic [14], enabling stable computation of the DHCS input (i.e., input of IP 2) from the input of IP 1 (i.e., incomplete HSI to be inpainted). This will become clear in Section 2.3. Simply speaking, the required DHCS input is just some spectral/spatial averages of the hyperspectral data cube. As it turned out, though the data is incomplete, it is sufficient to well approximate such spectral/spatial averages, meaning that (A2) is satisfied.

3. (A3) obviously holds true as both DHCS and HI target to reconstruct the complete hyperspectral data cube.

Therefore, the HI problem can be solved under the IPT framework, by transforming it into another domain wherein the DHCS problem has been effectively solved, to be detailed in Section 2.3. This surprisingly yields very good inpainting performance.

2.3. Computing the DHCS Input

Summarizing what discussed in Sections 2.1 and 2.2, the remaining task is to compute the DHCS input [14] from the incomplete HSI data $\{[\boldsymbol{X}]_{m,\ell} \mid (m,\ell) \in \boldsymbol{\Omega}\}$. In this section, we briefly recall the adopted DHCS solver [14] for self-contained purpose, followed by computing its input arguments from the incomplete HSI.

Consider a region of interest (ROI) with $L_1 \times L_2$ pixels ($L = L_1 L_2$). In hyperspectral compressed sensing (HCS), the compressed measurement $\boldsymbol{y}$ (observable quantity) can be written as $\boldsymbol{y} = \boldsymbol{\Phi}\boldsymbol{x}$, where $\boldsymbol{x} \triangleq \text{vec}(\boldsymbol{X})$ (causal factor), and $\boldsymbol{\Phi} \in \mathbb{R}^{m\times n}$ is the encoding matrix (with $m \ll n$) that is defined in [14, Equation 1] as

$$\boldsymbol{\Phi} = \begin{pmatrix} \boldsymbol{I}_L \otimes \boldsymbol{D} \\ \boldsymbol{B}^T \otimes \boldsymbol{I}_M \end{pmatrix} \in \mathbb{R}^{(L+ML_h)\times(ML)}, \quad (1)$$

in which $L_h \triangleq \frac{L}{r_1 r_2}$ with integer-valued parameters $r_1, r_2 \in \mathbb{Z}_{++}$ satisfying $\frac{L_1}{r_1}, \frac{L_2}{r_2} \in \mathbb{Z}_{++}$, $\boldsymbol{D} \triangleq \boldsymbol{1}_M^T \in \mathbb{R}^{1\times M}$, and $\boldsymbol{B} \triangleq (\boldsymbol{I}_{L_2/r_2} \otimes \boldsymbol{1}_{r_2}) \otimes (\boldsymbol{I}_{L_1/r_1} \otimes \boldsymbol{1}_{r_1}) \in \mathbb{R}^{L\times L_h}$. The encoding matrix can be generalized if higher sampling rate is allowed [14, Section III]. The meaning of $\boldsymbol{\Phi}$ will become clear as we talk about its associated decoder, which is to solve the DHCS inverse problem defined in [14, Equation (3)], i.e.,

$$\widehat{\boldsymbol{x}} = \quad (2)$$
$$\arg\min_{\widetilde{\boldsymbol{x}}} \|\boldsymbol{y}_p - (\boldsymbol{I}_L \otimes \boldsymbol{D})\widetilde{\boldsymbol{x}}\|_2^2 + \|\boldsymbol{y}_h - (\boldsymbol{B}^T \otimes \boldsymbol{I}_M)\widetilde{\boldsymbol{x}}\|_2^2,$$

where $\boldsymbol{y}_p \triangleq [\boldsymbol{y}]_{1:L}$ is the first part of $\boldsymbol{y}$, and $\boldsymbol{y}_h = [\boldsymbol{y}]_{L+1:L+ML_h}$ is the second part.

Therefore, the HSI $\boldsymbol{X}$ (or, equivalently, $\boldsymbol{x} = \text{vec}(\boldsymbol{X})$) can be reconstructed as $\widehat{\boldsymbol{x}}$ if (A1)-(A2) discussed in Section 2.1 are satisfied. Specifically, (A1) requires effective solver for (2), while (A2) requires computing/approximating the input arguments $(\boldsymbol{y}_p, \boldsymbol{y}_h)$ of (2), respectively discussed below:

- By carefully examining the operator $(\boldsymbol{I}_L \otimes \boldsymbol{D})$, it is actually a spectral averaging operator that averages the M spectral bands of $\boldsymbol{x}$, leading to a spectrally downsampled panchromatic (or multispectral) image $\boldsymbol{y}_p$. Though the spectral dimension is downsampled, the spatial information is retained in $\boldsymbol{y}_p$, and the first decoding term in (2) is to extract the spatial information from $\boldsymbol{y}_p$. Similarly, by analyzing the operator $(\boldsymbol{B}^T \otimes \boldsymbol{I}_M)$, it is actually a spatial averaging operator. Specifically, the L-pixel HSI $\boldsymbol{x}$ is partitioned into L_h superpixels, each containing $r_1 \times r_2$ pixels. The operator $(\boldsymbol{B}^T \otimes \boldsymbol{I}_M)$ is to average the $r_1 \times r_2$ pixel vectors in each superpixel of $\boldsymbol{x}$, leading to a spatially blurred HSI $\boldsymbol{y}_h$ (containing L_h blurred pixels). Though the spatial dimension is blurred, the spectral information is retained in $\boldsymbol{y}_h$, and the second decoding term in (2) is to extract the spectral information from $\boldsymbol{y}_h$. To summarize, (2) aims at reconstructing the HSI $\widehat{\boldsymbol{x}}$ from its spectrally downsampled version $\boldsymbol{y}_p$ (retaining spatial details) and spatially blurred version $\boldsymbol{y}_h$ (retaining spectral details), and this decoder (2) can be recast as a regularized coupled nonnegative matrix factorization (CNMF) problem solved under convex optimization (CO) framework, leading to the CO-CNMF algorithm [15] that is a highly effective decoder as demonstrated in [14]. So, (A1) is satisfied.
- From the above discussion, it is not difficult to see that the ℓth pixel of $\boldsymbol{y}_p$ is essentially the average of the M entries in $\boldsymbol{x}_\ell \in \mathbb{R}^M$, which can be directly computed if $\boldsymbol{x}_\ell$ is completely acquired. If $\boldsymbol{x}_\ell$ is incomplete, such an average can still be naturally approximated by the average of the observable quantities/entries in $\boldsymbol{x}_\ell$, i.e., $\{[\boldsymbol{X}]_{m,\ell} \mid (m,\ell) \in \boldsymbol{\Omega}\} \mid_{\ell \text{ is given}}$. Similarly, as illustrated above, each pixel in $\boldsymbol{y}_h$ is the average of $r_1 \times r_2$ pixels in $\boldsymbol{X} = [\boldsymbol{x}_1, \ldots, \boldsymbol{x}_L]$, which can be directly computed if all the $r_1 \times r_2$ pixels are acquired. In case that some of the $r_1 \times r_2$ pixels are missing, such an average can still be performed by ignoring those missing quantities. The above approximation strategies are expected to be effective due to the spatial/spectral smoothness in typical HSI. For example, in $\boldsymbol{y}_p$, because the number of spectral bands M is large when comparing to the number of missing bands in a given pixel in typical HI scenario [12, 18], the approximated averaging value should be good given the spectral smoothness [19]. So, (A2) is satisfied.

We conclude this section by the following remark. Unlike conventional random-projection-based HCS methods (e.g., Bernoulli/Gaussian random measurement matrices), the input of the adopted deterministic DHCS

solver is relatively easy to be obtained or approximated. We will experimentally demonstrate that the simple approximation strategy in the proposed IPT-based HI method (IPT-HI) works well even when there are nearly 25% incompletely acquired bands.

3. EXPERIMENTAL RESULTS

In this section, we compare the proposed IPT-HI with some benchmark HI methods, including 3D-PDE [10], FastHyIn [12], BPFA [9] and the low-rank matrix factorization via total-variation regularization (LRTV) proposed in [20], all implemented on Mathworks MATLAB R2019a. Our experiment was conducted on an urban hyperspectral data, widely studied in remote sensing area [21, 22]. The studied subscene contains 210×210 pixels, each covering a spatial area of 2×2 m^2. This Urban HSI covers 210 spectral bands with 10 nm spectral resolution, corresponding to wavelengths ranging from 0.4 to 2.5 μm. The channels 1-4, 76, 87, 101-111, 136-153 were removed due to dense water vapor and atmospheric effects, and the remaining 162 channels are used in the experiment.

Fig. 2. Pseudo-color image of the studied urban data.

For this HI experiment, we generate the data based on a practical scenario. Owning to small relative errors in the calibration of each detector and to the temporal variation of the detectors' response, a series of stripes would appear in the along-track direction, so we corrupt the studied HSI by serious stripes at different locations in the first 40 bands over a total of 162 (around 25%); cf. Figure 3(a). The corrupted HSI was fed into the studied HI methods for reconstructing the complete HSI, and the results are respectively shown in Figures 3(b) to 3(f), where one can see that IPT-HI has successfully reconstructed the spatial details.

To quantitatively evaluate the reconstruction performance, we adopt the peak signal-to-noise ratio (PSNR), spectral angle mapper (SAM), universal image quality index (UIQI) [23] and *erreur relative globale adimensionnelle de synthèse* (ERGAS). Rigorous definitions of PSNR, SAM , and ERGAS can be found from [15], while that of UIQI can be found from [13]; due to space limitation, they are not recalled here. Also, computational time (in seconds) is shown as an index of computational efficiency, which is based on the computer facility equipped with Core-i7-8700 CPU with 3.20-GHz speed and 16-GB random access memory. Please refer to [24] for related complexity analysis. The results are displayed in Table 1. One can see that BPFA has strong HI performance at the cost of significantly higher computational time, while, among the other peer methods, the proposed IPT-HI has best HI performance in terms of all the three indices. This demonstrates the potential of the IPT framework.

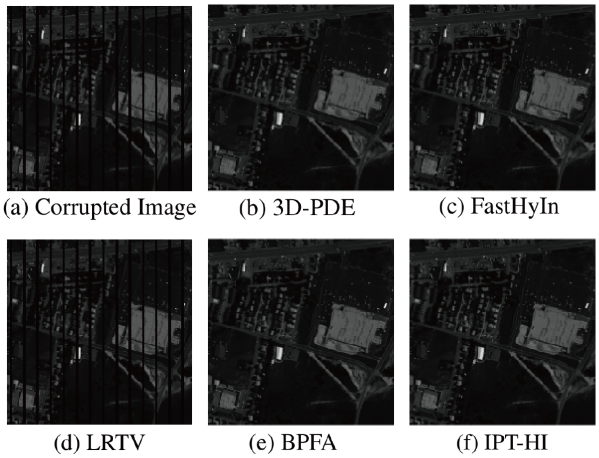

(a) Corrupted Image (b) 3D-PDE (c) FastHyIn

(d) LRTV (e) BPFA (f) IPT-HI

Fig. 3. Band 12 of the corrupted image (a) and its reconstructions by (b) 3D-PDE, (c) FastHyIn, (d) LRTV, (e) BPFA, and (f) the proposed IPT-HI.

Table 1. Quantitative assessment of HI methods.

Methods	PSNR (↑)	SAM (↓)	UIQI (↑)	ERGAS (↓)	TIME
3D-PDE	45.55	0.5113	0.9978	0.7256	4.49
FastHyIn	48.78	0.3978	0.9990	0.5240	7.64
LRTV	25.61	5.7391	0.7861	8.1284	84.88
BPFA	58.14	0.1768	0.9998	0.1864	6348.88
IPT-HI	53.12	0.2939	0.9996	0.3186	4.62

4. CONCLUSION

We have introduced a new concept called inverse problem transform (IPT), and apply IPT to solve hyperspectral inpainting (HI) by transforming HI into another inverse problem, i.e., decoding in hyperspectral compressed sensing (DHCS). Though directly solving HI using the observable but incomplete image (OII) is

challenging, it is straightforward to transform OII into the required inputs of an effective deterministic DHCS method, whose output is then the desired complete hyperspectral image. This idea of IPT surprisingly yields superior HI results, demonstrating its potential of being applied to solve other challenging inverse problems in the future whenever (A1)-(A3) hold.

5. REFERENCES

[1] H. Akbari, *et al.*, "Detection and analysis of the intestinal ischemia using visible and invisible hyperspectral imaging," *IEEE. Trans. Biomed. Eng.*, vol. 57, no. 8, pp. 2011–2017, Aug. 2010.

[2] J. M. Bioucas-Dias, *et al.*, "Hyperspectral remote sensing data analysis and future challenges," *IEEE Geosci. Remote Sens. Mag.*, vol. 1, no. 2, pp. 6–36, Jun. 2013.

[3] E. Villeneuve, *et al.*, "Nonlinear deconvolution of hyperspectral data with MCMC for studying the kinematics of galaxies," *IEEE Trans. Image Process.*, vol. 23, no. 10, pp. 4322–4335, Oct. 2014.

[4] D. Hong, *et al.*, "An augmented linear mixing model to address spectral variability for hyperspectral unmixing," *IEEE Trans. Image Process.*, vol. 28, no. 4, pp. 1923–1938, Apr. 2019.

[5] D. Hong, *et al.*, "Cospace: Common subspace learning from hyperspectral-multispectral correspondences," *IEEE Trans. Geosci. Remote Sens.*, vol. 57, no. 7, pp. 4349–4359, Jul. 2019.

[6] D. Hong, *et al.*, "Learnable manifold alignment (lema): A semi-supervised cross-modality learning framework for land cover and land use classification," *ISPRS J. Photogramm. Remote Sens.*, vol. 147, pp. 193–205, Jan. 2019.

[7] Y.-C. Hung, *et al.*, "Penetrating terahertz hyperspectral unmixing via Löwner-John ellipsoid: An unsupervised algorithm," submitted to IRMMW-THz, Buffalo, NY, USA, Nov. 13-18, 2020.

[8] G. Aubert, *et al.*, *Mathematical Problems in Image Processing: Partial Differential Equations and the Calculus of Variations*, vol. 147, Springer Science & Business Media, 2006.

[9] M. Zhou, *et al.*, "Nonparametric Bayesian dictionary learning for analysis of noisy and incomplete images," *IEEE Trans. Image Process.*, vol. 21, no. 1, pp. 130–144, Jan. 2011.

[10] J. D'Errico, "Inpainting nan elements in 3-d," MATLAB Central File Exchange. MathWorks, Natick, MA, USA, 2008, [Online]. Available: `https://www.mathworks.com/matlabcentral/fileexchange/21214-inpainting-nan-elements-in-3-d`.

[11] D. Knowles, *et al.*, "Infinite sparse factor analysis and infinite independent components analysis," in *Proc. ICA*, London, UK, Jun. 2010, pp. 381–388.

[12] L. Zhuang, *et al.*, "Fast hyperspectral image denoising and inpainting based on low-rank and sparse representations," *IEEE J. Sel. Top. Appl. Earth Obs. Remote Sens.*, vol. 11, no. 3, pp. 730–742, Mar. 2018.

[13] C.-H. Lin, *et al.*, "An explicit and scene-adapted definition of convex self-similarity prior with application to unsupervised Sentinel-2 super-resolution," *IEEE Trans. Geosci. Remote Sens.*, vol. 58, no. 5, pp. 3352 – 3365, May. 2020.

[14] C.-H. Lin, *et al.*, "A new hyperspectral compressed sensing method for efficient satellite communications," in *Proc. IEEE SAM*. Hangzhou, China, June 8-11, 2020.

[15] C.-H. Lin, *et al.*, "A convex optimization-based coupled nonnegative matrix factorization algorithm for hyperspectral and multispectral data fusion," *IEEE Trans. Geosci. Remote Sens.*, vol. 56, no. 3, pp. 1652–1667, Mar. 2018.

[16] C.-H. Lin, *et al.*, "A fast hyperplane-based minimum-volume enclosing simplex algorithm for blind hyperspectral unmixing," *IEEE Trans. Signal Process.*, vol. 64, no. 8, pp. 1946–1961, Apr. 2016.

[17] C.-H. Lin, *et al.*, "Maximum volume inscribed ellipsoid: A new simplex-structured matrix factorization framework via facet enumeration and convex optimization," *SIAM J. Imaging Sci.*, vol. 11, no. 2, pp. 1651–1679, Jun. 2018.

[18] M. Wang, *et al.*, "LRR-based hyperspectral image restoration by exploiting the union structure of spectral space and with robust dictionary estimation," in *Proc. IEEE ICIP*, pp. 4287–4291. Beijing, China, 2017.

[19] R. N. Clark, *et al.*, "USGS digital spectral library splib06a: U.S. Geological Survey, Digital Data Series 231," [Online]. Available: `http://speclab.cr.usgs.gov/spectral.lib06`, 2007.

[20] W. He, *et al.*, "Total-variation-regularized low-rank matrix factorization for hyperspectral image restoration," *IEEE Trans. Geosci. Remote Sens.*, vol. 54, no. 1, pp. 178–188, Jan. 2015.

[21] "HYDICE Urban hyperspectral data cube," [Online]. Available: `http://www.tec.army.mil/hypercube`.

[22] F. Zhu, *et al.*, "Spectral unmixing via data-guided sparsity," *IEEE Trans. Image Process.*, vol. 23, no. 12, pp. 5412–5427, Nov. 2014.

[23] Z. Wang, *et al.*, "A universal image quality index," *IEEE Signal Process. Lett.*, vol. 9, no. 3, pp. 81–84, Mar. 2002.

[24] C.-H. Lin, *et al.*, "All-addition hyperspectral compressed sensing for metasurface-driven miniaturized satellite," *accepted by IEEE Trans. Geosci. Remote Sens.*